# Geological Setting

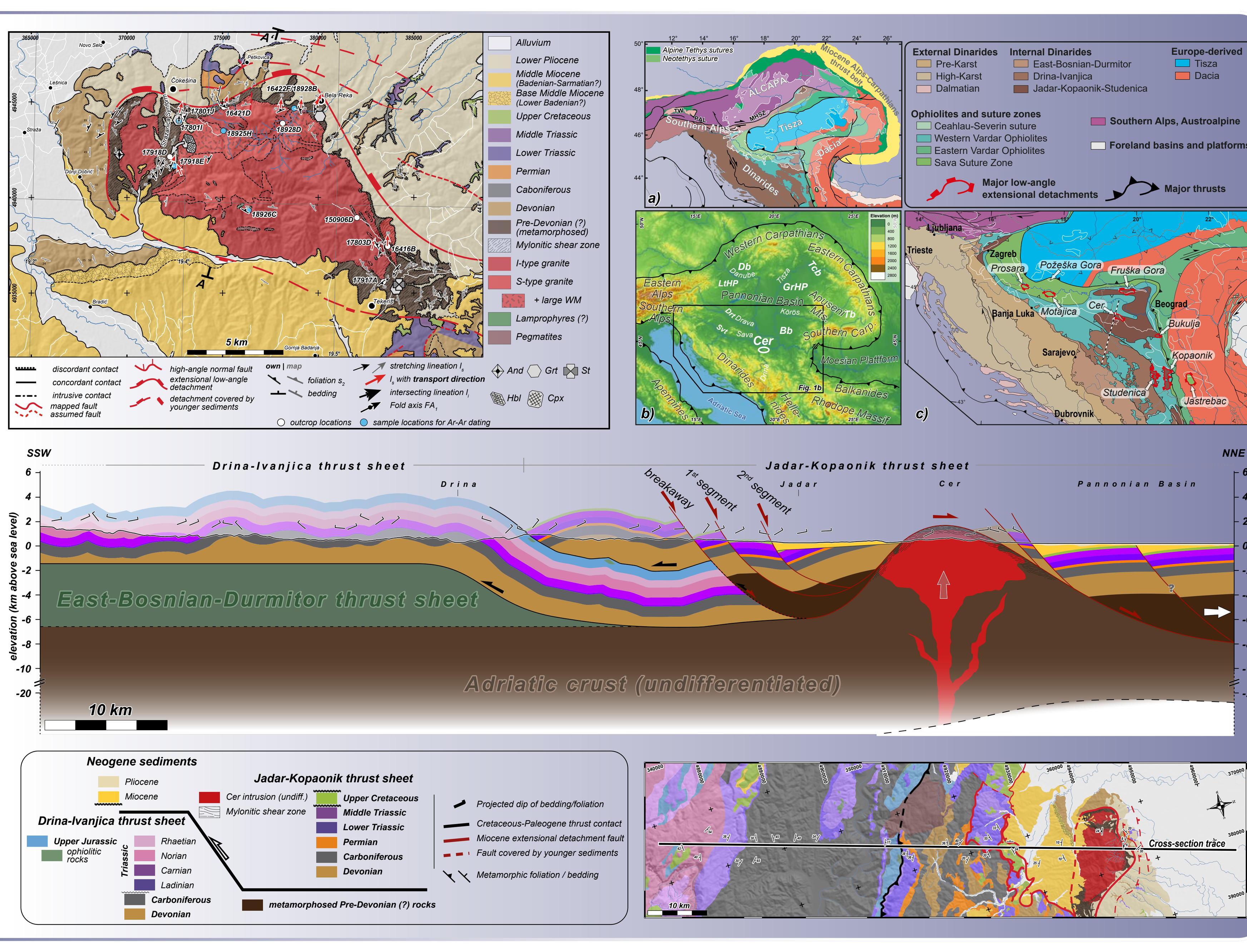

(a) Simplified overview map of major tectonic units and fault zones of the Alps-Carpathians-Dinarides region (modified after Schmid et al., 2020). MHSZ, Mid-Hungarian shear zone; PAL, Periadriatic line; TW, Tauern window. Shaded area depicts extent of the Pannonian Ba-sin.

(b) Digital Elevation map (based on SRTM data with 90 m resolution) of the Pannonian Basin and surrounding orogens with their respective deformation fronts. Abbreviations (white bold italic) indicate major subbasins of the Pannonian Basin system: Bb, Banat Basin; Db, Danube basin; Drt, Drava trough; GrHP, Great Hungarian Plain; LtHP, Little Hungarian Plain; Svt, Sava trough; Tb, Tran-sylvanian basin; Tcb, Transcar-pathian basin.

(c) Tectonic units of the Dinarides and neigh-boring regions (modified after Schmid et al., 2020) with locations of metamorphic core com-plexes and asso-ciated low-angle detachment faults in red. The dashed line depicts the locati-on of the cross section trace (Fig. 12).

(d) Geological map of Cer metamorphic core complex (MCC) based on the Yugoslavian map sheets "Zvornik" and "Vladimirci", 1:100000 (WGS84, UTM Zone 34N, Filipović (1971); Mojsilović et al. (1975)), supplemented by own observations. Grey structural elements are adopted from the Yugoslavian maps.

(e) Balanced cross-section through the Cer metamorphic core complex (MCC) and the southerly adja-cent nappe contact between the Jadar-Kopaonik thrust sheet in the north and the Drina-Ivanjica composite nappe in the south. Upper Jurassic strata are composed of W-Vardar ophiolites and as-sociated mélange. The breakaway fault that roots in the low-angle extensional shear zone border-ing the Cer MCC reactivates the ramp-segment of the nappe contact.

# Microstructures and petrography

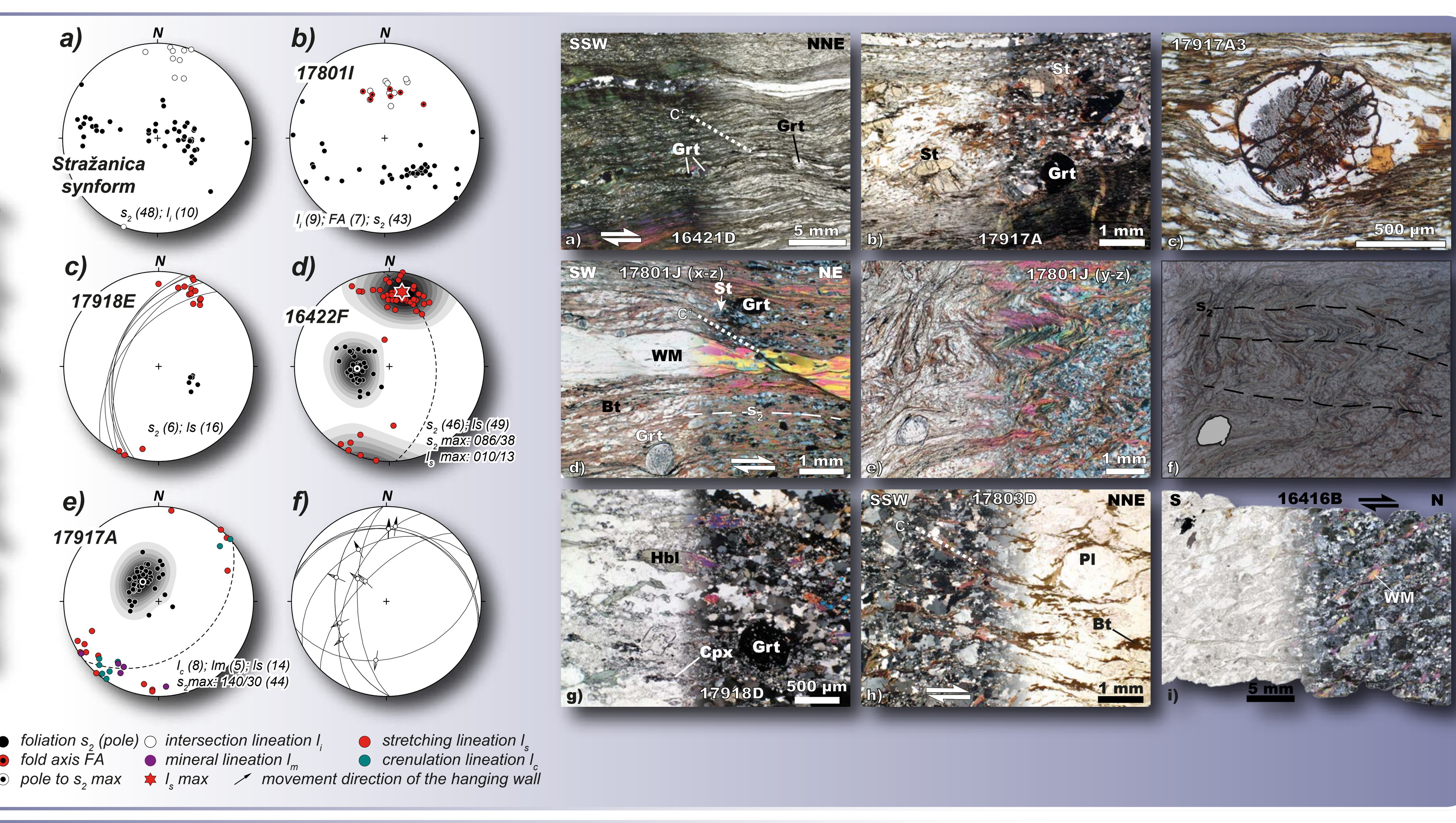

**Left:**
Stereographic projections (equal area, lower hemisphere) of structural data from various parts of the Cer MCC: (a) mylonitic shear zone within the central Stražanica synform; (b) northern Stražanica synform; (c) S-type granite at the eastern limb of the Stražanica synform with kinematic indicators showing top-N transport; d) mylonites at the northeastern margin of Cer MCC; e) structural data collected north of Teke-ris; f) brittle fault planes with slip lineations from the magmatic core of Cer MCC.

**Right:**
Thin section photomicrographs of igneous and metamorphic rocks from Cer MCC under plane- and cross-polarized light (for locations of the corresponding outcrops see above).
a) Garnet-bearing mica schist developing C'-ty-pe shear bands that indicate top-N transport;
b) garnet-staurolite-bearing micaschist from the south-eastern part of Cer (Tekeriš);
c) Detailed view of Grt from (b) exhibiting snow-ball structure that indicate syntectonic growth; d) mylonitic garnet- and staurolite-bearing mica-schist from the northern Stražanica-synform, extensional shear bands that developed in s2 indicate top-N transport;
e-f) y-z- section of the same sample reveals a folded s1-foliation, resulting in the axial-planar s2-foliation;
g) garnet- and pyroxene-bearing hornblen-de-hornfels with mylonitic s2 foliation (Stražani-ca-synform);
h) monzodiorite with metamorphic foliation composed of biotite that developed C'-type shear bands, indicating top-N transport;
i) deformed, garnet-bearing S-type granite. Prekinematic white mica forming mica fish and S-C-fabric indicate top-N sense of shear.

# $^{40}Ar/^{39}Ar$-Geochronology

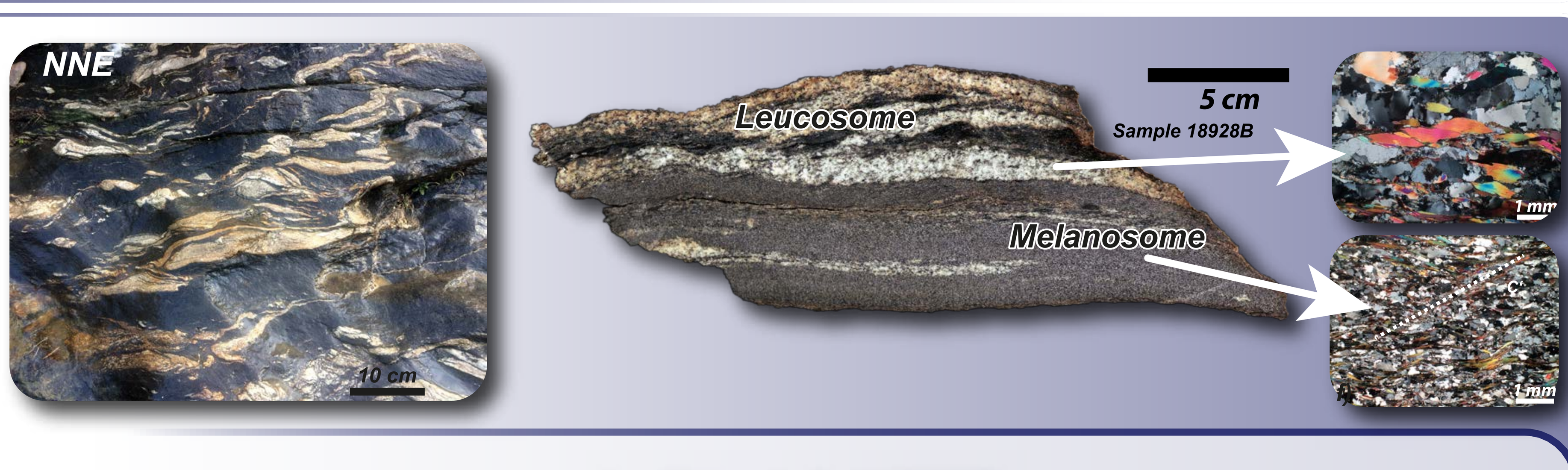

**Top:**
Outcrop 16422F near Bela Reka exposing injected migmatites, i.e. injected leucosomes in a melanocratic host rock.
Detailed view of sample 16422F1 and 18928B (used for Ar-Ar in-situ LA-NGMS and sing-le-grain total fusion/step heating analyses).
Asymmetric boudins and the nebulous occurren-ce of leucocratic material in the lower left.
Thin section micrographs of the leucosome and melano-some of the rock. Note that only relics of biotite are present in the leucosome. Both domains show mica fish and C'-type shear bands.

## In-Situ LA-NGMS

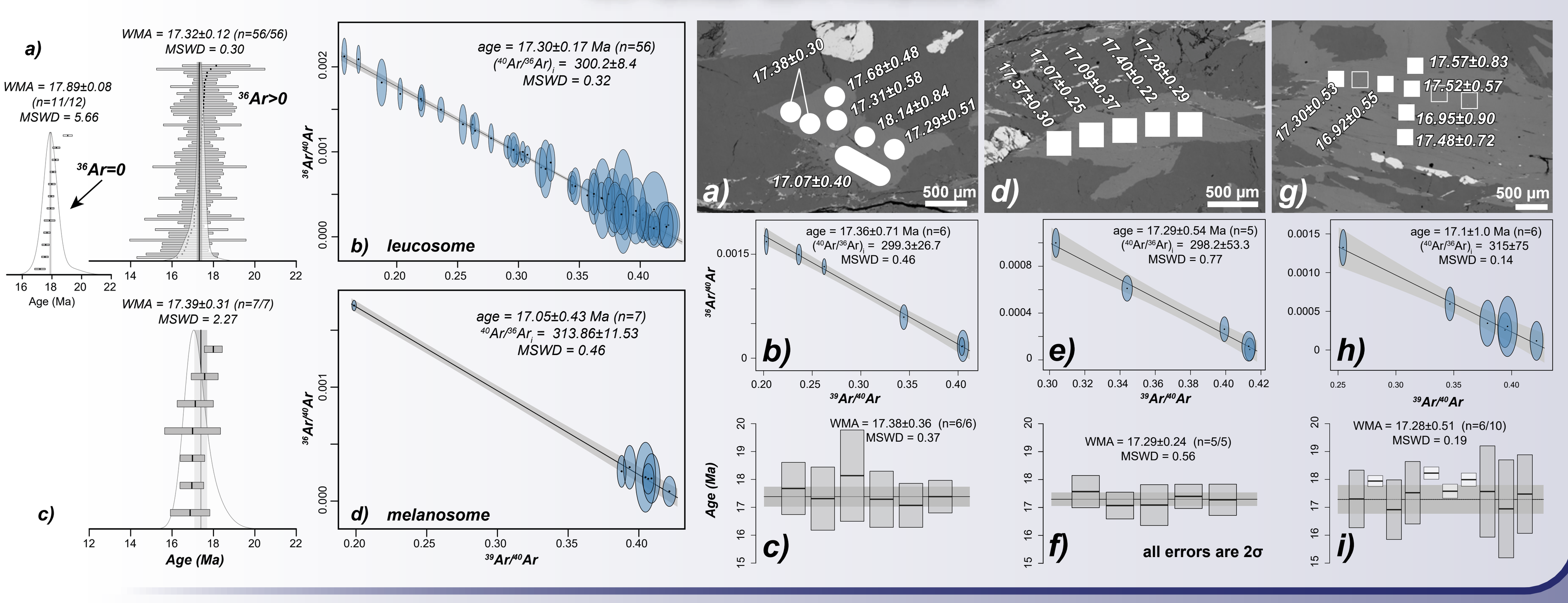

**Bottom:**
**Left:** Rank order plots with weighted mean ages (WMA) and inverse isochron plots of white mica (sam-ple 16422F1) obtained by in-situ laser ablation dating. Analytical uncertainties are shown on a 95% confidence level. MSWD, mean square of weighted deviates.
a) Data with and without atmospheric correction due to 36Ar signals below the detection limit. The lack of atmospheric correction leads to a weighted mean age that is significantly older than the WMA of aliquots corrected for atmo-spheric Ar.
b) Inverse isochron plot of the same spot analy-ses as shown in a) of the leucosome.
c-d) WMA and IIA plot of white mica of the mela-nosome.
**Right:** Examples of intra-granular dating of white mica from the low-angle shear zone (sample 16422F1) with BSE images showing spot sites (top row; filled: with atmospheric correction, empty: no atmospheric correction due to $^{36}Ar$ signal below detection limit) and inverse isochron plots and weighted mean ages (middle and bottom row, respectively). Note that the ages without atmospheric correc-tion (white bars in (i)) are slightly older (too much $^{40}Ar$) and have lower uncertainties (no propagation of the uncertainty of the $^{36}Ar$ signal into the final age).

## Multi-grain step heating

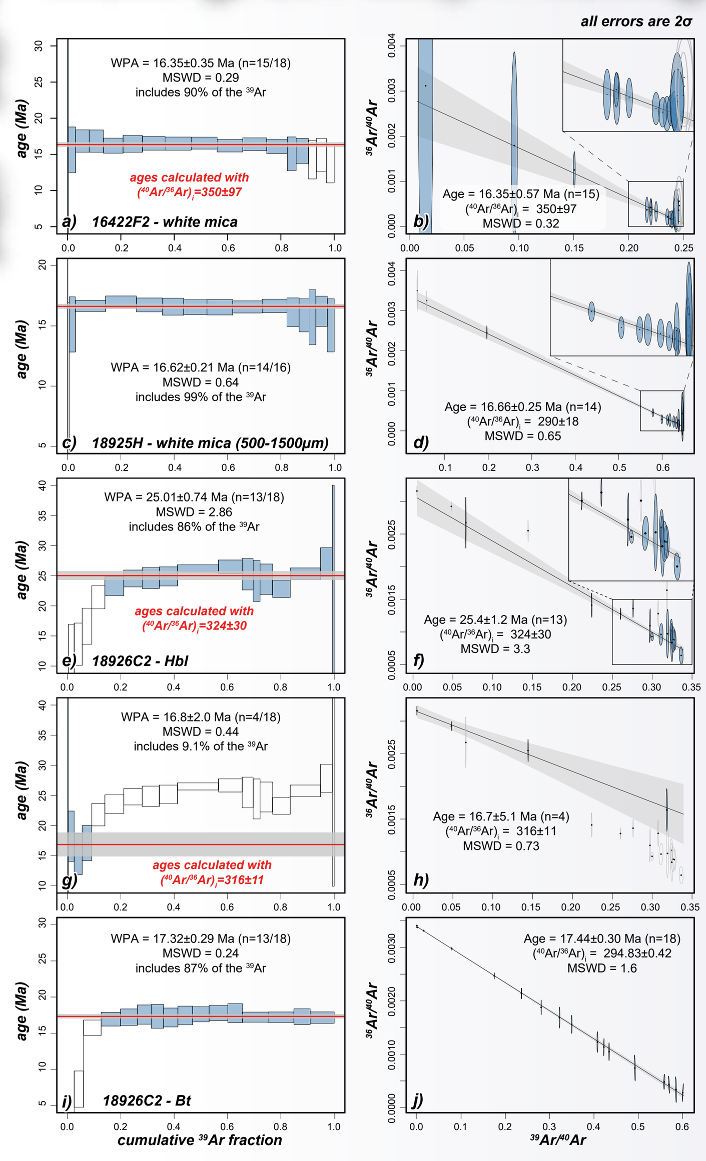

## Single-grain total fusion/step heating

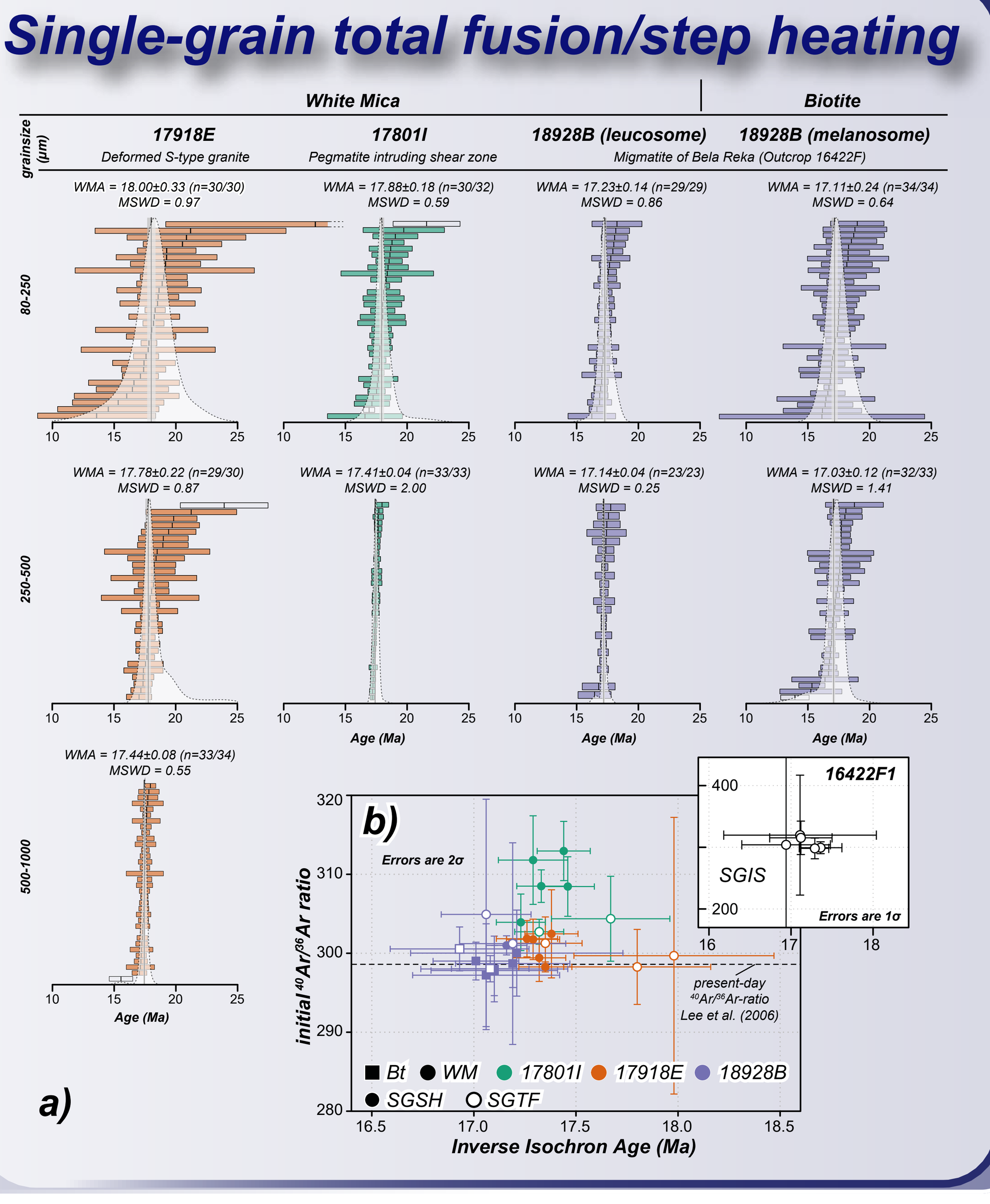

**Left: conventional step heating**
Age spectra and inverse isochron plots of step-heating experiments.
**a-b)** White mica from a boudined leucosome of the low-angle shear zone.
**c-d)** White mica from an undeformed S-type granite below the shear zone (18925H).
**e-f)** Amphibole from I-type granitoid (18926C2).
**g-h)** Recalculation of the age spectrum in (e) with an initial $^{40}Ar/^{36}Ar$-ratio of 316±11, deter-mined by the inverse isochron through the first four steps (h).
**i-j)** Biotite from the same sam-ple (18926C2). The age spectrum indicates Ar-loss for the low-temperature steps.

**Right: SGTF/SGSH**
**(a)** Rank order plots of single-grain total fusion ages obtained on white mica and biotite for differ-ent grain sizes. WMA, weighted mean age (confidence interval=95%, corresponding to 1.96 σ); MSWD, mean square of weighted deviates. Empty bars are outlier which were excluded from the calculation of the weighted mean ages. Dashed curves show the corresponding Kernel density es-timates.
**(b)** Initial $^{40}Ar/^{36}Ar$-ratios of single-grain total fusion (SGTF; same data as in (a), inverse isochron plots in Fig. S1) and single-grain step-heating experiments (SGSH; Fig. S2). Inset: same plot type as (b), but for single-grain in-situ measurements (SGIS) of 5 WM grains.

# Conclusions

***The opening of the Pannonian Basin in response to slab-re-treat underneath the Carpathi-an orogen also affected the Dinarides***

***Miocene extension in the Pan-nonian Basin also affected the distal Adriatic margin, where (in the case of Cer) the reacti-vation of nappe contacts as low-angle detachment sys-tems resulted in the exhumati-on of mid-crustal core com-plexes such as Cer MCC at approx. 17-18 Ma.***

***Extension was most pronoun-ced in the internal Dinarides and involved the reactivation of former suturing thrusts of the Sava zone as low-angle detachments, shown by Ustaszewski et al. (2010).***

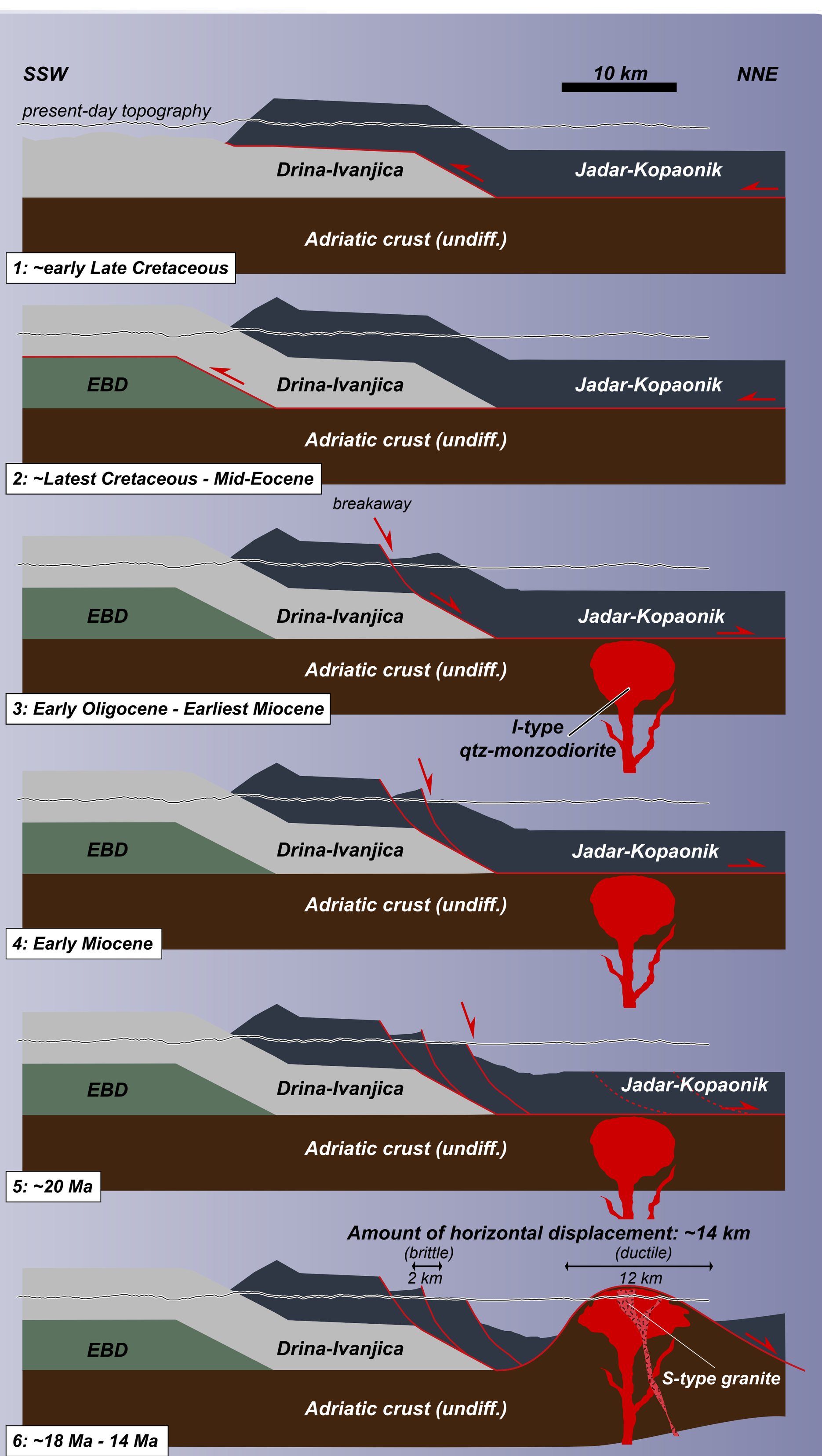

**Top:**
Conceptual kinematic model along a SSW-NNE-oriented transect, illustrating the evolution of the most internal part of the Dinari-des since early Late Cretaceous times, post-da-ting the obduction of the western Vardar ophioli-tes. These ophiolites are considered as the uppermost part of the re-spective thrust sheets. Red arrows and lines depict areas of active deformation; black lines those of inactive defor-mation.

1) Thrusting of Jadar-Kopaonik unit onto Drina-Ivanjica (DI) unit.

2) In-sequence thrusting of DI onto the East Bosnian-Durmitor (EBD) unit.

3) Emplacement of I-type in-trusion at ~32 Ma. Early Miocene onset of extension (Pannonian Basin peak extension at ~19 Ma) with reactivati-on of the ramp segment of the former thrust contact as a low-angle normal fault.

4-5) Continuing extension along listric normal faults rooting in a flat detachment along the former thrust plane.

6) Denudation and isostatic uplift of continental crust followed by the intru-sion of the S-type granite. Continuing exhumation of Cer MCC.

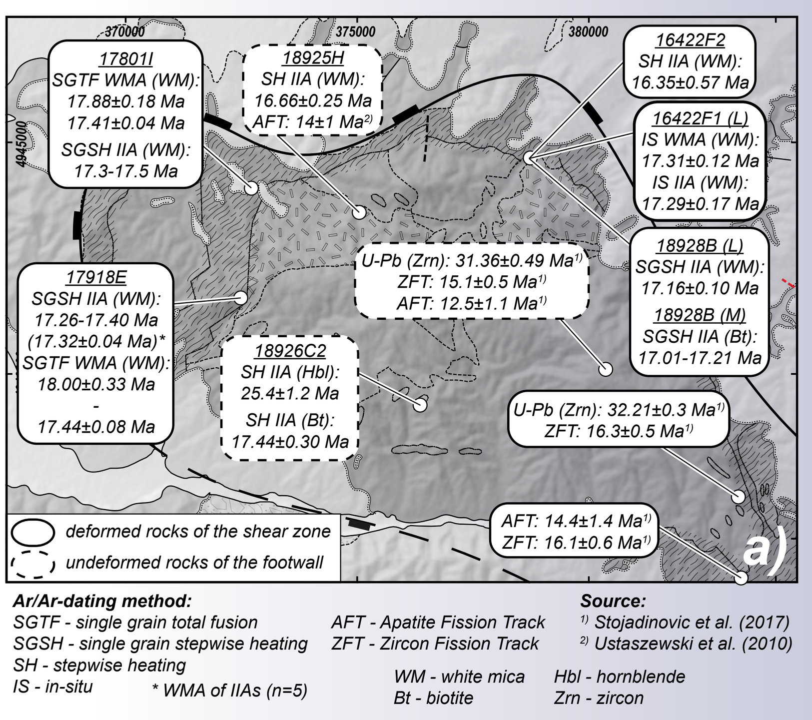

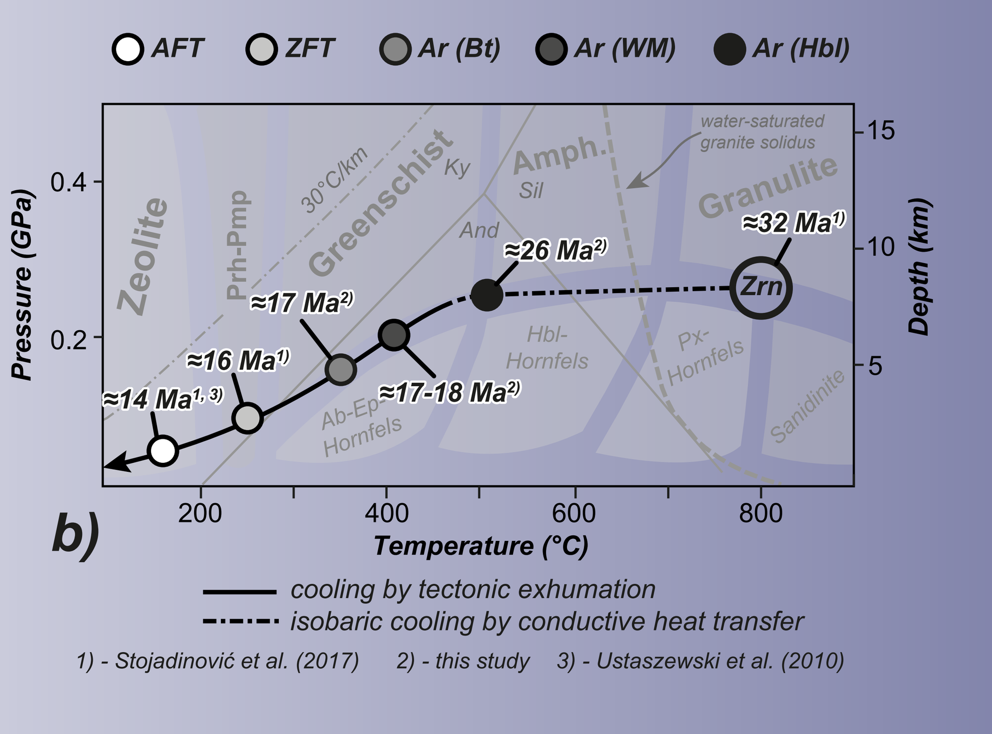

**Bottom:**
**a)** Geochronological data from the Cer massif, own data and published ones, with data from the shear zone in solid boxes and the the undefor-med footwall in dashed boxes. WMA, weighted mean age; IIA, inverse isochron age; L, leucoso-me; M, melanosome.

**b)** Interpretative P-T-t path of the Cer Massif and surrounding metamorphic rocks. Intrusion of the I-type granitoid at ~32 Ma is followed by isobaric cooling until c. 20 Ma and final cooling by tecto-nic denudation.

*The supplementary Material can be accessed* ***here!***